

**Squeezing water from a stone: H₂O in nominally anhydrous minerals
from granulite xenoliths and deep, hydrous fractional crystallization**

Emily J. Chin¹, Sean T. Curran¹, and G. Lang Farmer³

¹Geosciences Research Division, Scripps Institution of Oceanography, University of California, San Diego, La Jolla, CA, USA

²Department of Geological Sciences and CIRES, University of Colorado Boulder, CO, USA

Corresponding author: Emily J. Chin (e8chin@ucsd.edu)

Key Points:

- H₂O contents in cpx, opx, garnet in Proterozoic lower crustal xenoliths from Colorado
- Mineral H₂O content used to reconstruct bulk rock and calculate melt H₂O
- Xenoliths represent metamorphosed igneous cumulates from high-P, hydrous magmas

Abstract

Although ~10% of Earth's water resides within continents, H₂O distribution throughout the continental lithosphere and partitioning of H₂O in nominally anhydrous minerals (NAMs) remain poorly constrained. Models of continent formation and destruction depend on H₂O content. We report H₂O contents in NAMs measured *in situ* on petrographic thin sections by secondary ion mass spectrometry (SIMS) of Proterozoic deep crustal xenoliths from Colorado, USA. Clinopyroxene, orthopyroxene, and garnet contain average H₂O contents of 560, 347, and 85 ppm, respectively; reconstructed bulk rock H₂O ranges from ~75 to ~600 ppm. Inter-mineral H₂O ratios overlap experimental mineral/melt D values, and are used to calculate H₂O of melts last in equilibrium with the xenoliths. We propose that these xenoliths represent cumulates fractionated from a primitive, hydrous (≥ 1 wt.% H₂O) melt at high (~1 GPa) pressures, similar to conditions in modern subduction zones, and potentially associated with widespread arc accretion that formed the core of North America in the Precambrian.

1 Introduction

Water is key to plate tectonics on Earth, which, in turn, is vital to the production of continental crust. Yet debate continues over when plate tectonics and arc-related continental crust formation began, with estimates ranging widely from as late as 800 Ma to as early as ~4 Ga (Arndt, 2013). Processes such as intraplate/plume magmatism and accretion of oceanic plateaus have thus been proposed in contrast to the arc model of continental growth (Rudnick, 1995). An important aspect of this debate involves the formation and evolution of lower continental crust – particularly, the nature of magmas that first encounter the Moho prior to further differentiation, and the solids such magmas leave behind. The budget and trajectory of magmatic water in the deep crust has profound consequences for cumulate mineralogy, lower crustal rheology, and ultimately bulk crustal composition. For instance, higher magmatic water expands the liquidus field of pyroxene over plagioclase (Kushiro & Yoder, 1969), resulting in pyroxenite cumulates dominating arc lower crust, compared to plagioclase-rich cumulates in oceanic lower crust (Chin et al., 2018). Water also plays an important role in crusting melting (Collins et al., 2020). Lastly, even at ppm levels, water in mineral lattices can significantly enhance crystal plasticity and decrease rock viscosity (Hirth & Kohlstedt, 1995), thereby promoting deformation, and may thus contribute to de-stabilization of dense, mafic crust and the survival of buoyant, felsic continental crust.

Knowledge of the initial water content of primary magmas should allow us to discern whether continental crust formed via a hydrous process (subduction) versus anhydrous processes (plumes, ridges), because water content of primary magmas is an important discriminator for subduction vs. non-subduction settings (Sobolev & Chaussidon, 1996). The problem is that determining the water content of a primary magma is challenging, because such magmas are rarely, if ever, directly sampled. An alternative perspective is provided by deep crustal xenoliths that represent early fractionated magmatic cumulates or restites. Because they are denser than melts, cumulates are left behind in the deep crust, preserving a record of early magmatic processes. Such a record is obscured in shallowly emplaced magmas that traverse, and potentially assimilate, thick and heterogeneous crust. Primitive crystalline solids (cumulates) fractionated from magmas offer a glimpse into the trace element and volatile content of melts these cumulates were last in equilibrium with (Chin et al., 2018), if the partitioning of trace elements and volatiles between cumulate minerals and melt is known, and if such cumulates were not later re-hydrated or metasomatized.

We propose the following testable hypotheses wherein deep crustal cumulates could be used to distinguish initially hydrous melts versus anhydrous melts, thus using such cumulates to discriminate tectonic setting. In a subduction zone, primary magmas start wet – already containing at least ~2 wt. % H₂O (Plank et al., 2013). Subsequent fractional crystallization evolves more hydrous derivative melts that have been shown to fractionate garnet and clinopyroxene-rich cumulates in the lower crust (Lee et al., 2006; Muntener & Ulmer, 2006) and amphibole-rich cumulates in the middle crust (Davidson et al., 2007). Igneous cumulates and restites are increasingly recognized as an important driver for refining continental crust to silica-rich compositions, particularly if such cumulates contain large amounts of garnet to render them convectively unstable (Lee & Anderson, 2015), allowing them to founder, leaving behind less dense, Si-rich crust. Relics of lower crustal foundering may exist in cumulates that deformed by high-temperature plastic deformation, or may have been deformed when the lithosphere thickened to pressures high enough to stabilize garnet (Chin et al., 2016). By contrast, in a non-subduction setting such as a plume, primary melts would be predicted to be drier compared to melts generated in subduction zones, due to larger extent of melting, which

81 would dilute the initial H₂O content of mantle-derived melts. Water contents of primary
82 intraplate magmas are highly variable, spanning the entire range from MORB-like to arc-
83 like (Liu et al., 2017); this may stem from heterogeneity of deep mantle reservoirs.
84 Cumulates that fractionate from flood basalts appear to fall along tholeiitic trends
85 dominated by olivine fractionation (Rehfeldt et al., 2007). In addition, igneous cumulates
86 might exhibit limited evidence of plastic deformation if they formed in a plume setting
87 (Tommasi & Ishikawa, 2014).

88 Here, we address the interrelated issues of the hydration state of the lower continental
89 crust and continental crust formation processes by examining a suite of granulite
90 xenoliths from the Devonian-age State Line Kimberlite District, northern Colorado, USA.
91 Our samples are ideal for constraining the water content of stable continental lower crust
92 because they record Proterozoic crustal formation ages, and, importantly, erupted well
93 before the Cenozoic Laramide Orogeny, which is thought to have caused a widespread
94 hydrous overprint of the deep lithosphere beneath Western North America (Jones et al.,
95 2015; Li et al., 2008). An evaluation of previously published bulk rock major element
96 data, combined with new clinopyroxene major element data and H₂O contents in NAMs
97 analyzed by secondary ion mass spectrometry (SIMS) suggests that the State Line
98 xenoliths could represent deep crustal cumulates, rather than restites or crystallized
99 basaltic melts. We go a step further and propose that the melt that crystallized the
100 protoliths of the State Line xenoliths was hydrous (≥ 1 wt.% H₂O), based on calculated
101 H₂O contents of liquids last in equilibrium with the xenoliths. A plausible scenario for
102 such a melt could have been subduction magmatism associated with the Yavapai arc
103 terrane, one of several Proterozoic arc building blocks of the North American continent.

2 Geologic setting & previous work

2.1 Geologic background

The State Line Kimberlite District comprises ~100 kimberlite diatremes of Devonian age, a large number of which bear mantle and lower crustal xenoliths (Eggler et al., 1987). The diatremes were emplaced within Proterozoic continental crust of the

Colorado Province (Bickford et al., 1986), just south of the boundary with Archean crust of the Wyoming Craton (**Fig. 1**). The Wyoming Craton and Medicine Hat Block represent part of a number of Archean cratonic cores amalgamated in the Paleoproterozoic to form the nucleus of Laurentia (Whitmeyer & Karlstrom, 2007). Starting at ~1.8 Ga, a series of oceanic terranes and island arcs accreted to the southern edge of the Wyoming Craton. These accreted arc terranes form large scale, northeast-trending belts with juvenile crust ages decreasing away from the cratonic core: the

Yavapai Province (1.7 – 1.8 Ga), the Mazatzal Province (1.7 – 1.6 Ga), and the Granite-

Rhyolite Province (1.55 – 1.35 Ga). The core of the North American continent coalesced completely by ~1.0 Ga (the Grenville Orogeny).

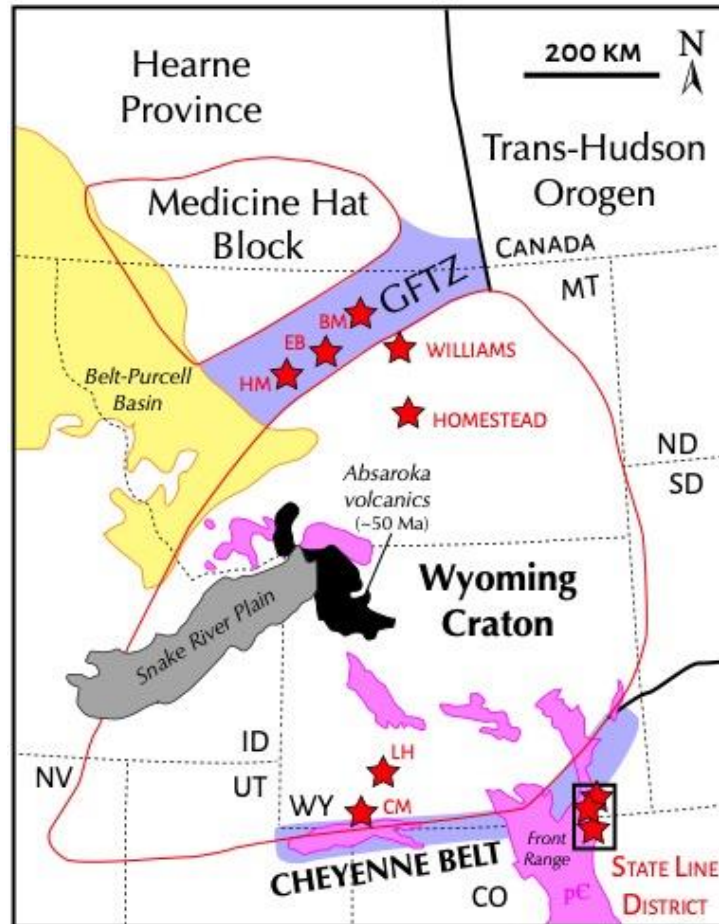


Fig. 1. Geologic & tectonic setting. Simplified map of the Wyoming Province showing key geologic features. Xenolith localities are denoted by red stars: BM = Bearpaw Mountains, EB = Eagle Butte, HM = Highwood Mountains, CM = Cedar Mountain, LH = Leucite Hills. GFTZ = Great Falls Tectonic Zone.

The Colorado Province remained quiescent until the end of the Paleozoic, when regional deformation developed the Ancestral Rocky Mountains. The next major tectonic event to impact the Colorado Province did not occur until ~70 Ma with the Laramide Orogeny, classically attributed to low angle subduction of the Farallon Plate beneath Western North America (Dickinson & Snyder, 1978). Low angle subduction induced significant fluid metasomatism and hydration of the deep lithosphere across much of the Western US (Humphreys et al., 2003). The impact of deep lithospheric hydrous metasomatism is manifested by amphibole and biotite-rich lower crustal xenoliths erupted in 3.0 to 0.89 Ma lamproites (Lange et al., 2000) to the northwest of the Devonian-age State Line kimberlites (Leucite Hills; **Fig. 1**), as well as distinctive geochemical signatures in Cenozoic volcanic rocks throughout the southwestern US ascribed to melting of hydrous metasomatized continental lithosphere (Farmer et al., 2020). Importantly, the xenoliths from the State Line kimberlites do not show evidence for hydrous metasomatism (Farmer et al., 2005), and their Devonian eruption ages means they were never impacted by the hydrous overprint of the Laramide Orogeny. Thus, the State Line lower crustal xenoliths represent a potentially pristine glimpse of the water content of lower continental crust preserved since its formation.

2.2 Lower crustal xenoliths

Lower crustal xenoliths from the State Line District include a variety of mafic lithologies, but are dominated by (nominally anhydrous) mafic granulites, with subordinate amphibolites, anorthosites, and gabbroic xenoliths (Bradley & McCallum, 1984; Farmer et al., 2005). Within the mafic granulites, Bradley and McCallum (1984) defined three groups: two pyroxene granulites, two pyroxene garnet granulites, and clinopyroxene garnet granulites. The final equilibration conditions of garnet-bearing granulites range from ~1 – 1.5 GPa and ~700 – 800 °C (Farmer et al., 2005). In addition, xenoliths of mantle eclogite are common (Ater et al., 1984). Although most of these eclogitic xenoliths are eclogites *sensu stricto* (e.g., containing omphacitic clinopyroxene), a small number of xenoliths were also classified as “eclogite” by Farmer et al. (2005) (e.g., sample SH-E1), but as we discuss later in this paper, some of these previously classified eclogites do not resemble MORB-eclogites *sensu stricto*. Generally speaking, garnet-bearing granulites are compositionally gradational to eclogites (Ater et al., 1984;

Bradley & McCallum, 1984). For example, Bradley and McCallum (1984) noted that the mafic garnet-clinopyroxene granulites have relatively high jadeite content in their clinopyroxenes, similar to the sodic clinopyroxenes in the eclogite xenoliths, suggesting a gradual transition into eclogite facies. Here, we will refer to the aforementioned three groups of nominally anhydrous mafic granulites collectively as “lower crustal xenoliths” and divide them into two broad groups based on mineralogy: garnet-free and garnet-bearing. No “true” eclogites from Ater et al. (1984), nor amphibolites, are examined in this paper.

The modal mineralogy of the State Line lower crustal xenoliths is dominated by clinopyroxene, orthopyroxene, plagioclase, and garnet; these phases constitute >90% by volume of most of the xenoliths (Bradley & McCallum, 1984). Amphibole is present in some 2-pyroxene granulites (Bradley & McCallum, 1984; Farmer et al., 2005), but is absent or rare in garnet-bearing xenoliths. The most common accessory minerals are ilmenite, rutile, and apatite. Farmer et al. (2005) also reported minor amounts of zircon, barite, and K-feldspar. The latter two minerals were interpreted as grain boundary contaminants from the host kimberlite, as observed in K-rich phases along grain boundaries and K-feldspar occasionally replacing plagioclase grains.

U-Pb ages of zircons from State Line lower crustal xenoliths show a wide range of dates, with a dominant population of $^{207}\text{Pb}/^{206}\text{Pb}$ dates of 1.73 to 1.6 Ga (Farmer et al. 2005). This age population overlaps the Yavapai Orogeny (1.71 – 1.68; Whitmeyer and Karlstrom (2007)). There are also smaller populations of zircons with Archean ages (presumably inherited, and only present in amphibolites), ages ~1.4 Ga ages, as well as with ages coeval with the kimberlite eruption (Farmer et al., 2005). Unsurprisingly, zircons are rare in the more mafic xenoliths (e.g. the garnet-bearing, two-pyroxene lithologies). The oldest ages recorded by zircons in the mafic xenoliths are ~1.72 Ga, with evidence of overprinting (deduced from sector zoning (Farmer et al., 2005)). In summary, Farmer et al. (2005) interpreted the U-Pb age systematics of the State Line xenoliths to largely reflect lower crustal growth during the Paleoproterozoic, with metamorphic zircon overgrowths occurring at 1.3 – 1.4 Ga, coeval with the widespread regional metamorphic event at that time in North America.

3 Methods

3.1 Secondary ion mass spectrometry

We analyzed H₂O by ion microprobe in nominally anhydrous minerals *in situ* in petrographic thin sections. New one-inch round thin sections were made from previously collected xenolith material. Prior to thin section preparation, each billet was microdrilled and a grain of commercially available Suprasil glass (H₂O content 0.99 ± 0.36 ppm; E. Hauri, personal communication) was embedded in a central area of the xenolith (**Fig. 2b**), ensuring a completely flat and well-polished surface. The purpose of the Suprasil is to monitor the instrumental H₂O background, a critical factor due to the ubiquitous presence of volatile-rich epoxy in petrographic thin sections and the typically low H₂O concentrations of nominally anhydrous minerals.

To minimize the background, prior to analysis the ion microprobe was baked for ~2 days to attain ultra-high vacuum of $\sim 2 \times 10^{-10}$ torr. During a session, four thin sections, plus a separate block with mineral standards, were simultaneously introduced into the airlock at $\sim 5 \times 10^{-9}$ torr for at least 4 days, and in some cases up to 7 days, to ensure complete degassing of extraneous H₂O. Analyses were obtained using a CAMECA 7f-Geo SIMS, with the following operating parameters: primary Cs⁺ beam with current of 4.5 – 5 nA, accelerating voltage of 10 kV, rastered over a 20 x 20 μm area with a field aperture limiting the secondary ion collection area to an 8 μm spot in the center of the rastered area. Each analysis comprised of 2 min of pre-sputtering then 30 cycles through the mass sequence ¹²C, ¹⁶O¹H, ¹⁸O, ¹⁹F, ²⁷Al, Cl and ³⁰Si. OH (or H₂O) was determined by using a mass resolving power of ~5200 to separate ¹⁶O¹H from ¹⁷O; H₂O concentrations were determined using calibration curves (**Supporting Information**) developed using mineral standards from (Aubaud et al., 2007; Mosenfelder et al., 2011; Mosenfelder & Rossman, 2013a, 2013b). During analyses, the ion image and counts were monitored at all times, and any visible “hot spots” in the ion image (presumably corresponding to tiny, hydrous inclusions or cracks) were noted, and corresponding cycles deleted if necessary. ¹²C was used as a monitor for contamination and/or cracks. Any measurements with high levels of ¹²C, ¹⁹F, or visible perturbations in the ion image were not reported.

Owing to the wide range of Si in minerals analyzed (garnet, pyroxene, plagioclase, amphibole, apatite, phlogopite), in order to minimize matrix effects we normalized masses to ^{18}O , since the O contents of most silicate minerals are very similar (in contrast to Si which can vary by tens of weight %). Estimation of uncertainties followed the protocol outlined in Chin et al. (2016), and ranged from 10 to 15% (2 RSE). Over the course of two analytical sessions, the average H_2O background ranged between ~15 and ~20 ppm; we background-corrected all analyses using an average value of 23 ppm.

3.2 Electron microprobe analysis

Major element composition of pyroxenes, garnet, plagioclase, amphibole, and phlogopite were analyzed by electron microprobe using a CAMECA SX100 at Brown University (accelerating voltage 15 kV, beam current 20 nA, spot size 1 μm). In-house mineral standards and secondary mineral standards were used for calibration. Relative standard deviation was <1 % for major elements and ~5 % for minor elements.

3.3 EDS mapping

Energy dispersive spectroscopy (EDS) maps were obtained for selected thin sections using an FEI Apreo LoVac field emission gun scanning electron microscope (SEM) at UC San Diego. Operating parameters were an accelerating voltage of 20 kV, beam current of 3.2 nA, and 250 μs dwell time.

3.4 EBSD

Electron backscatter diffraction (EBSD) maps of selected thin sections were obtained with an Oxford Instruments Symmetry EBSD detector on an FEI Apreo LoVac field emission gun (SEM) at UC San Diego. Thin sections were not carbon-coated prior to analysis, and maps were run in low vacuum mode. Automated EBSD maps were obtained using a step size of 5 μm , working distance between 26 – 28 mm, and accelerating voltage of 20 kV. Raw EBSD data were first cleaned using Oxford HKL CHANNEL5 software by removing wild spikes, followed by filling of non-indexed pixels down to 5 nearest neighbor pixels. Typically, cleaning was minimal as most indexing rates were 90% or higher. The cleaned EBSD data were then processed in the open source MTEX software to produce various types of crystal orientation maps (IPF, mis2mean, GOS) and pole figures.

Sample ID	Rock type	Petrographic notes	Mineral modes
2-pyroxene granulites			
SD2-LC75	2-px granulite [†]	Medium-grained subhedral granoblastic	[26% cpx, 16% opx, 56% plag, trace oxides] ¹
SD2-LC118	2-px granulite [†]	Medium-grained subhedral granoblastic; very similar texturally and mineralogically to SD2-LC75	
NX4-LC2	2-px granulite [†]	Medium-grained subhedral granoblastic	
2-pyroxene garnet granulites			
SD2-LC120	2-px gt granulite [†]	Medium- to coarse-grained anhedral granoblastic orthopyroxene and plagioclase, with interstitial clinopyroxene and ilmenite and rutile. Garnet occurs throughout in fine-grained clusters (resembling foam), as well as in weakly developed coronas around orthopyroxene. Rutile grains are subrounded and medium-grained.	[35% plag, 30% opx, 25% gt, 10% cpx, minor ilmenite and K-feldspar, trace rutile and zircon] ²
SD2-LC71	2-px gt granulite [†]	Medium- to coarse-grained anhedral granoblastic Plagioclase contains deformation twins Garnet and clinopyroxene show a coarse myrmekitic texture organized into loosely defined coronas	[35% cpx, 12% opx, 29% gt, 23% plag, trace oxides] ¹
NX4-LC1	2-px gt granulite [†]	Medium-grained subhedral granoblastic Weak foliation defined by alignment of elongated opx, cpx, ilmenite [†] Ilmenites are widely distributed; garnet coronas appear to have nucleated predominantly on ilmenite grains Plagioclase contains deformation twins	
Opx-free garnet granulite			
SD2-LC74	Cpx-gt granulite [†]	Medium- to coarse-grained subhedral granoblastic Garnet shows various textures, from fine-grained, foamy clusters (symplectites) to coarse grains near ilmenite and clinopyroxene	[30% cpx, 30% gt, 35% plag, 3% ilm, minor K-feldspar, trace apatite, rutile, zircon, barite] ²
Xenoliths with <5 % plagioclase			
SH-E1	Eclogite [†]	Nearly bi-mineralic, very coarse-grained Large, round rutile grains dispersed throughout	[50% cpx, 48% gt, 2% rutile] ³
SD2-L110	2-px gt granulite	Resembles bi-mineralic granulites/eclogites petrographically Medium-grained subhedral granoblastic, weakly foliated with foliation defined by pyroxene or garnet-rich bands; some bands composed almost exclusively of coarse-grained clinopyroxene Plagioclase occurs interstitially between garnet and pyroxene Garnet-cpx coronas are either very small and fine-grained or absent	[40% cpx, 15% opx, 40% gt, 1% apatite, 3% plag, 1% phlogopite, trace oxide] ³
Medium grained = 1 to 5 mm; Coarse grained = >5 mm [†] classified by Farmer et al. 2005 ¹ calculated using least squares inversion of the whole-rock composition, if available (from Farmer et al. 2005) and average mineral compositions ² from Farmer et al. 2005 ³ determined by pixel counting of whole-thin section SEM EDS maps in Adobe Photoshop			

Table 1. Xenolith descriptions, petrography, and modal mineralogy.

4 Data and Results

4.1 Mineralogy and petrography

Although previous studies (Bradley & McCallum, 1984; Farmer et al., 2005) reported three distinct mineral assemblages in the State Line lower crustal xenolith suite, here we will broadly describe the xenoliths as two groups: garnet-free and garnet-bearing (**Table 1**). Garnet-free (i.e., two-pyroxene granulite) xenoliths are characterized by equigranular texture and numerous grains meeting at 120° triple junctions, exemplified in SD2-LC75 (**Fig. 2d**). Mineral modes are dominated by plagioclase (~70%), with subequal amounts of clinopyroxene and orthopyroxene (~25-30% total pyroxene), and ~3-5% ilmenite. In contrast, garnet-bearing xenoliths vary widely in mineral modes and textures (**Fig. 2**). Many garnet-bearing xenoliths have garnet-clinopyroxene coronas formed around ilmenite and plagioclase (Farmer et al., 2005). Below, we highlight notable features of three garnet-bearing xenoliths that encompass the mineralogical and textural complexity of the lower crustal xenolith suite.

SH-E1 (**Fig. 2a**) (classified as an eclogite by Farmer et al. (2005)) is very coarse-grained (>1 cm) and comprised of approximately equal amounts of clinopyroxene and garnet, with ~2% rutile. Clinopyroxene grains are often bent and deformed. Rutile occurs as 0.15 to 1.5 mm grains with various morphologies ranging from euhedral to rounded. Garnet occurs as very large (1 – 3 cm) grains with irregular, interlobate grain boundaries with clinopyroxene-occupied embayments.

SD2-L110 (**Fig. 2b**) contains ~40% clinopyroxene, ~40% garnet, ~15% orthopyroxene, ~5% plagioclase + K-feldspar, ~1% apatite, and minor ilmenite, phlogopite, and hornblende. Clinopyroxene occasionally forms coarse-grained, equant bands (**Fig. 2b**). Apatite is dispersed widely throughout the xenolith but is less abundant in clinopyroxene-rich bands (**Fig. 2e, f**). Garnet-clinopyroxene coronas are uncommon and small in size.

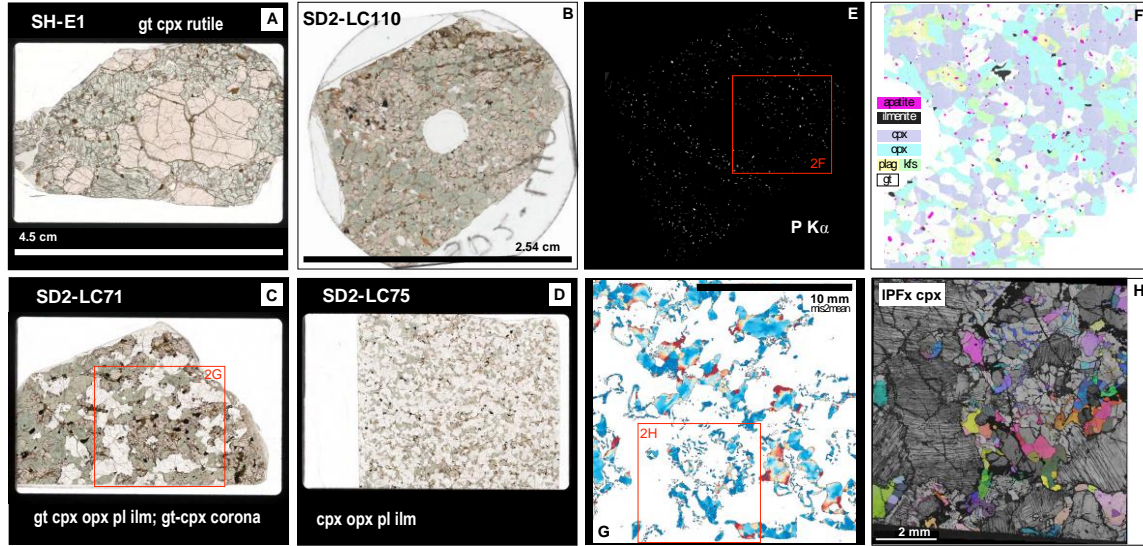


Fig. 2. Representative petrographic and microtextural features of the State Line lower crustal xenoliths. Left 4 panels (**A-D**): plane-polarized light scans of thin sections. (**B**) shows an example of a 1-inch round thin section with Suprasil glass mounted in the center for SIMS analyses (standard size thin sections are shown for other xenoliths because more area is available for observation). Right panels (**E-H**): Microbeam maps of SD2-L110 and SD2-LC71. (**E**) is an EDS map of P highlighting the widespread distribution of apatite in xenolith SD2-LC110. (**F**) shows a false-color stacked EDS map of a sub-area of E. (**G**) is a mis2mean map of clinopyroxene grains from the red outlined area in (**C**). (**H**) is the same area in (**G**) mapped by EBSD (shown here is an inverse pole figure map of clinopyroxene, superimposed on band contrast, in the x sample direction). Note abundance of deformation twins in plagioclase, as well as the similarity in IPF colors of within-corona, fine-grained clinopyroxene but more random colors in coarser-grained clinopyroxene.

SD2-LC71 contains ~25% plagioclase, ~35% clinopyroxene, ~15% opx, ~20% garnet, ~3-5% ilmenite, and trace amounts of K-feldspar. A distinctive feature of SD2-LC71 is the widespread occurrence of garnet-clinopyroxene coronas (**Fig. 2g, h**), which may comprise up to 30% or more of the xenolith. Farmer et al. (2005) noted the abundance of garnet-clinopyroxene coronas in several State Line granulite xenoliths, and interpreted the coronas to form from precursor orthopyroxene and calcic plagioclase. The coronas are irregular and lack concentric, mineral-specific zoning often seen in typical granulites (McLelland & Whitney, 1980). Within coronas, clinopyroxene occurs as small, worm-like grains surrounded by garnet (**Fig. 2g, h**); outside coronas, clinopyroxene occurs either as rims around orthopyroxene or as large porphyroclasts (**Fig. 2c**).

In summary, the State Line garnet-free and garnet-bearing lower crustal xenoliths constitute a relatively simple mafic mineralogy, comprising two pyroxenes, plagioclase, ilmenite, and/or garnet. Olivine is absent. Garnet-bearing xenoliths show a greater diversity of textures and deformation microstructures compared to the garnet-free group. Some of these features, such as garnet-clinopyroxene coronas, attest to textural disequilibrium (Bradley & McCallum, 1984).

4.2 Deformation microstructures

Microstructures of two xenoliths, SD2-L110 and SD2-LC71, were investigated in detail using EBSD mapping. In SD2-L110, clinopyroxene and orthopyroxene define a foliation (**Fig. 3**) and exhibit measurable, but weak, crystallographic preferred orientations (CPOs) (**Fig. 3**). The CPOs of both clinopyroxene and orthopyroxene are similar: though weak, they show [001] maxima parallel to and [010] maxima perpendicular to the apparent lineation/trace of foliation (**Fig. 3**). Such CPOs suggest slip along [001] and (010) as glide plane, consistent with naturally deformed deep lithospheric enstatites (Avé Lallemant, 1969).

A similar macroscopic foliation, loosely defined by garnet and clinopyroxene, is also observed in SD2-LC71 (**Fig. 2c**). Large plagioclase grains record evidence of plastic deformation, as shown by deformation twins, some of which are bent (**Fig. 2h**). Garnet-clinopyroxene textures in SD2-LC71 appear to have formed by reaction (Farmer et al., 2005), as evidenced by intricate garnet-clinopyroxene coronas forming near and around orthopyroxene, plagioclase, and occasionally ilmenite. Note that garnet and

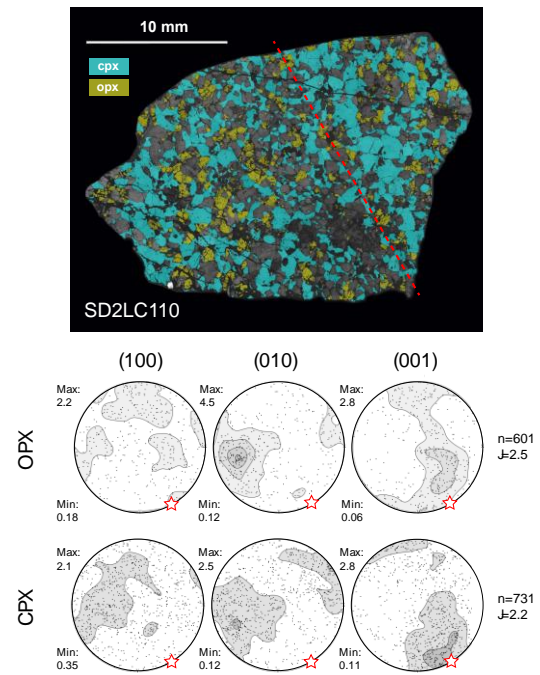


Fig. 3. Top: Large-area EBSD map of SD2-LC110. Only clinopyroxene and orthopyroxene are highlighted on top of band contrast. Dashed red line represents trace of foliation plane. Bottom: Pole figures (one point per grain) of orthopyroxene and clinopyroxene. N = number of grains, J = J index, a measure of the CPO strength.

clinopyroxene, together, constitute over 60% of the mineral mode (**Table 1**). Fine-grained corona clinopyroxene grains share similar crystallographic preferred orientations (based on inverse pole figure map, or IPF, in the sample reference frame; **Fig. 2h**) compared to coarser grained clinopyroxene outside coronas. Interestingly, large clinopyroxene porphyroclasts appear to have higher degrees of lattice distortion compared to fine-grained clinopyroxene in garnet coronas. This is shown in the mis2mean (misorientation to the mean) map in **Fig. 2g** and quantitatively in **Fig. 4**. The mis2mean measures the extent of intragranular misorientation by plotting the difference of orientation (misorientation) between the crystal's average orientation and the measured orientation at a given point in the grain. Since crystal misorientations generally arise from dislocations, mis2mean maps provide a graphical representation of the extent of ductile deformation in a grain population.

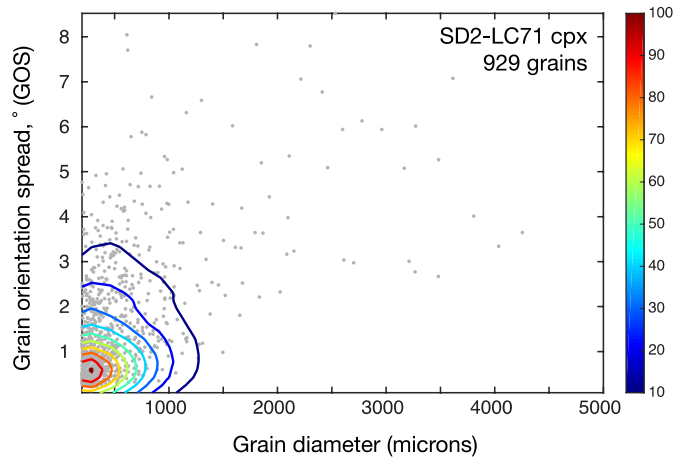


Fig. 4. Grain orientation spread (GOS) vs. grain size for 929 clinopyroxene grains in SD2-LC71. The GOS is similar to mis2mean, but reports 1 value for each grain denoting the degree of internal misorientation (higher numbers represent more intragranular misorientation). Each gray point represents 1 grain. The data have been contoured using a 2D histogram method to show that there are a large number of small grains with low GOS (these correspond to clinopyroxene inside garnet coronas) and a small number of large grains with high GOS (these correspond to clinopyroxene porphyroclasts).

4.3 Mineral compositions: major elements and water content

Clinopyroxene major element compositions from Bradley and McCallum (1984) and Farmer et al. (2005) along with new data from four xenoliths (SD2LC-110, SHE-1, SD2LC-71, SD2-LC75) are plotted against MgO in **Fig. 5**; all data are reported in **SI Table 1**. Clinopyroxenes are diopsidic with significant jadeitic components (Bradley & McCallum, 1984; Farmer et al., 2005) and generally unzoned with respect to major elements. The average H₂O content of clinopyroxene varies from 75 ppm to 760 ppm,

and is inversely correlated with clinopyroxene Mg# (**Fig. 6; Table 2**). H₂O contents are relatively homogeneous within individual grains within a given xenoliths, however some xenoliths show a range of H₂O concentrations across individual grains. Generally, grains are unzoned with respect to H₂O, but a few xenoliths show grains with slightly higher H₂O in cores versus rims.

We report new orthopyroxene major element compositions for SD2-LC75, SD2-LC71, and SD2-L110; these data as well as selected mineral data published in Bradley and McCallum (1984) and Farmer et al. (2005) are included in **SI Table 1**. Orthopyroxene is generally enstatitic (~70%) and unzoned with respect to major elements. Average H₂O content of orthopyroxene ranges from 233 to 410 ppm (**Table 2**).

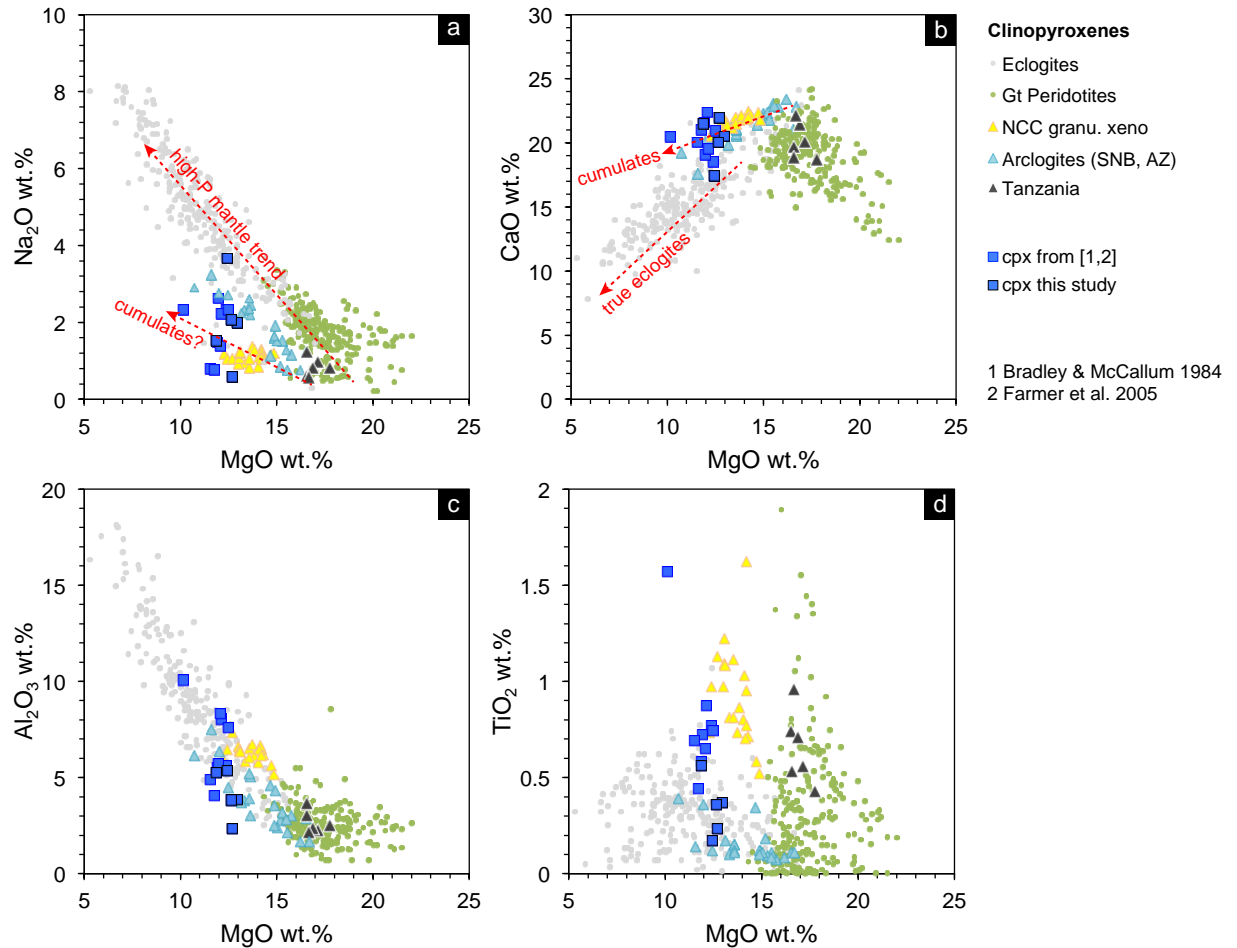


Fig. 5. Clinopyroxene compositions. Clinopyroxene major element oxides plotted against MgO (wt. %). Dashed red lines highlight general trends followed by mantle rocks (high-P mantle trend, exemplified by mantle eclogites) and distinct trend followed by cumulates. Compositions of clinopyroxenes in eclogite xenoliths are from Hills and Haggerty (1989), Fung and Haggerty (1995), Beard et al. (1996). Compositions of clinopyroxenes in garnet peridotites are from Boyd and Mertzman (1987), Ehrenberg (1982), Hervig et al. (1986), Franz et al. (1996), Reid et al. (1975). **(A)** Na₂O vs. MgO, **(B)** CaO vs. MgO, **(C)** Al₂O₃ vs. MgO, **(D)** TiO₂ vs. MgO

367

368 Major elements were analyzed in garnet from SD2-LC71, SH-E1, and SD2-L110 and
 369 reported in **SI Table 2**. Garnets are pyrope-almandine. The average H₂O content of
 370 garnet varies from 42 to 139 ppm and is also inversely correlated with bulk rock Mg# and
 371 clinopyroxene Mg#. Garnets are unzoned with respect to H₂O and also quite
 372 homogeneous in major element composition within individual grain populations in a
 373 given xenolith (**SI Table 2**).

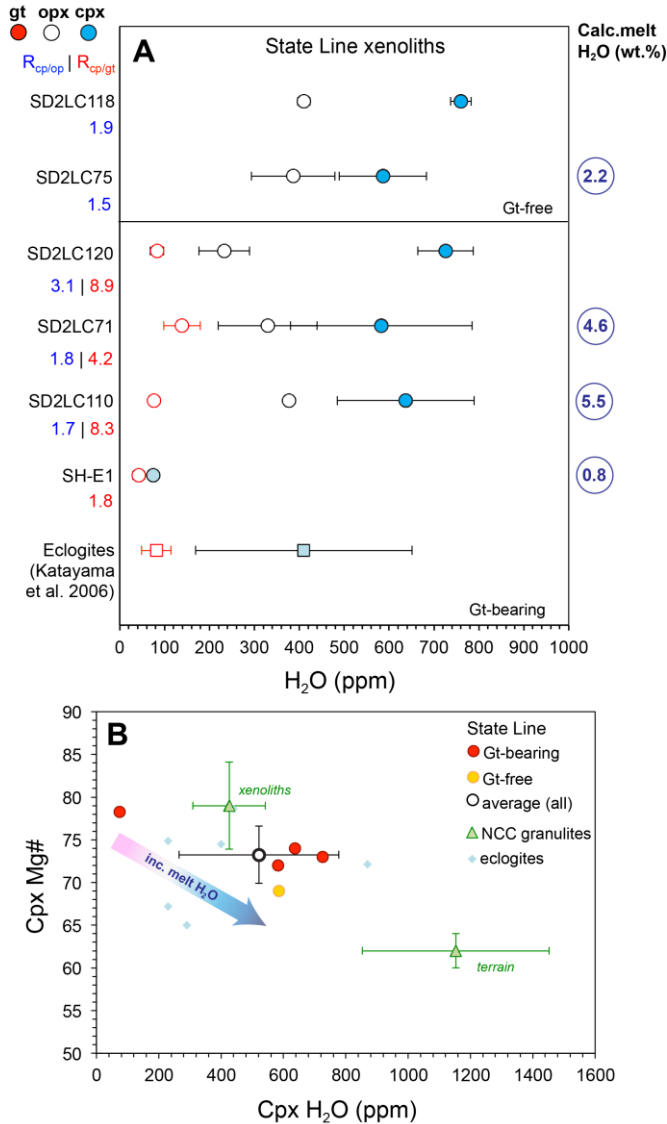


Fig. 6. Water content in major silicate nominally anhydrous minerals. H₂O (ppm) in garnet, orthopyroxene, and clinopyroxene in State Line lower crustal xenoliths. Inter-mineral ratios shown for cpx/opx and cpx/garnet on left side; calculated melt H₂O content shown on right side. See text for details. **(B)** Clinopyroxene Mg# vs. clinopyroxene H₂O (ppm). NCC granulite data from Yang et al. (2008); eclogite data from Katayama et al. (2006). Shaded arrow shows calculated trend of increasing melt H₂O with decreasing Cpx Mg#.

In addition to the modally abundant minerals clinopyroxene, orthopyroxene, and garnet, we also analyzed H₂O contents in accessory minerals apatite, phlogopite, and amphibole. These are reported in **SI Table 3**.

4.4 Whole rock major element systematics

Whole rock major element oxides of 15 xenoliths previously reported in Bradley and McCallum (1984) and Farmer et al. (2005) are plotted against Mg# (atomic Mg/(Mg+FeT)*100) in **Fig. 7a-d**. FeO_T and MgO are plotted against SiO₂ in **Fig. 7e** and **f**, respectively. Broadly, the State Line lower crustal xenoliths are mafic, with Mg#s ranging from 51 to 69. Average SiO₂ contents are slightly lower (48.7 wt. %) than

average MORB (50 wt.%). Notably, some xenoliths extend to low SiO_2 values <47 wt.% (Fig. 7c). The State Line xenoliths also trend towards lower CaO with decreasing Mg# compared to average MORB (Fig. 7e), and towards higher FeO with decreasing Mg#. We point out xenolith SH-E1, which was previously classified as MORB-type eclogite (Farmer et al., 2005) plots away from average MORB in terms of Al_2O_3 (10 wt.% compared to 15 wt.% for average MORB), MgO (13 wt.% vs 7.5 wt.%) and Na_2O (2.2 wt.% versus 2.6 wt.%) (Fig. 7).

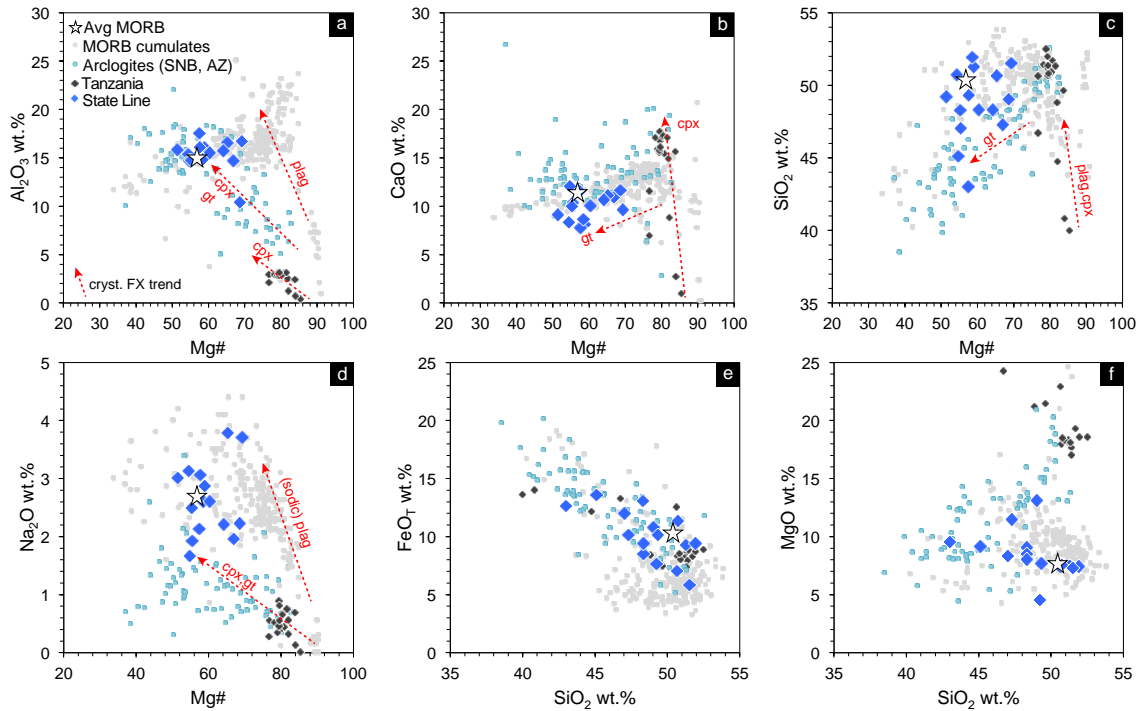


Fig. 7. Whole-rock major element systematics. Whole-rock major element oxides of State Line lower crustal xenoliths. Also plotted for comparison are average MORB, MORB cumulates, arclogites, intraplate rift cumulates (Tanzania). Dashed red lines are schematic trends corresponding to crystal fractionation of different minerals (plagioclase, clinopyroxene, etc.). **(A)** Al_2O_3 vs. Mg#, **(B)** CaO vs. Mg#, **(C)** SiO_2 vs. Mg#, **(D)** Na_2O vs. Mg#, **(E)** FeO_T vs. SiO_2 , **(F)** MgO vs. SiO_2

391

5 Discussion

5.1 Inter-mineral partitioning of H₂O

To assess equilibrium with respect to H₂O contents between minerals, we compare inter-mineral ratios of measured H₂O concentrations (“R”, **Table 2**) to experimental mineral/melt partition coefficients (“D”). Due to lack of published experimental H₂O partition coefficients for lower crustal rocks, we used experimental D values from Aubaud et al. (2004) and Tenner et al. (2009). Although these experiments pertain to mantle assemblages, our xenoliths have a broadly similar basaltic mineralogy, with the exception of olivine. We note, however, that published ranges of experimental H₂O mineral/melt partition coefficients are similar between plagioclase (0.001 – 0.006; Lin et al. (2019)) and olivine (0.0013 – 0.0021; Hauri et al. (2006)). Similar to mantle rocks, lower crustal rocks of broadly basaltic compositions contain abundant pyroxene, which has the highest DH₂O mineral/melt compared to olivine, plagioclase, and garnet. Thus, we can expect that H₂O partitioning between nominally anhydrous minerals in basaltic granulites to share some similarities with mafic and ultramafic upper mantle rocks.

		SHE1	SD2LC110	SD2LC71	SD2LC120	SD2LC75	SD2LC118
Garnet	Min	19	69	99	70		
	Max	67	102	230	104		
	Average	42	77	139	83		
	1 σ	13	9.9	41	15		
	n	6	2	9	7		
Cpx	Min	62	476	345	634	486	733
	Max	96	1225	1178	835	766	775
	Average	75	637	583	726	586	760
	1 σ	9.8	152	202	62	97	23
	n	11	9	11	3	5	2
Opx	Min		372	249	132	307	399
	Max		380	647	322	547	425
	Average		377	330	233	387	410
	1 σ		4.4	110	56	93	14
	n		2	6	3	4	3
	R cpx/opx (avg)		1.7	1.8	3.1	1.5	1.9
	R cpx/gt (avg)	1.8	8.3	4.2	8.7		
	Bulk H ₂ O ^a	58	406	291		242	
	Bulk H ₂ O ^b	82	651	564			
	(ppm)						
	Calc melt H ₂ O ^a	0.8	5.5	4.6		2.2	
	(wt.%)						
n = number of individual grains analyzed 1 σ = 1 standard deviation calculated from total number of individual spots per mineral (at least 3 spots per grain) ^a reconstructed using average mineral H ₂ O contents ^b reconstructed using maximum mineral H ₂ O contents							

Table 2. H₂O content (ppm) in NAMs, inter-mineral partitioning, and reconstructed bulk H₂O and calculated melt H₂O contents. n = number of individual grains analyzed; 1 σ = 1

standard deviation calculated from total number of individual spots per mineral (at least 3 spots per grain).^areconstructed using average mineral H₂O contents; ^breconstructed using maximum mineral H₂O contents.

Using average mineral water contents, R_{cpx/opx} for garnet-free xenoliths SD2-LC118 and SD2-LC75 are 1.9 and 1.5, respectively (**Fig. 6, Table 2**). These values agree well with D values of 1.4 ± 0.3 for a garnet-free basaltic assemblage at 1 – 2 GPa from Aubaud et al. (2004). R_{cpx/opx} (using average values) for garnet-bearing xenoliths SD2-LC120, SD2-LC71, and SD2-LC110 R_{cpx/opx} are 3.1, 1.8, and 1.7 (**Table 2**), which also overlap with the range of D_{cpx/opx} of 1.2 to 2 reported by Tenner et al. (2009) for garnet-bearing systems. Using average mineral water contents, R_{cpx/gt} range from 1.8 to 8.3 (**Table 2**). If the maximum values for cpx and garnet water content is used, R_{cpx/gt} range from 1.4 to 12. For comparison, experimental D_{cpx/gt} range from 5.5 to 14 as reported in Tenner et al. (2009).

While the R values between minerals in our xenoliths show decent overlap with experimental D's, the question arises as to whether the kimberlite eruption itself could have modified mineral H₂O concentrations. Addition of H₂O from the kimberlite magma into minerals was likely negligible, given that most individual mineral grains are homogeneous and unzoned with respect to H₂O. Furthermore, no correlation exists between mineral H₂O and grain size – if the host magma modified mineral H₂O, one might expect some correlation given that large grains should retain more H₂O and smaller grains either less H₂O (degassing) or gained H₂O (ingassing). A few clinopyroxene grains do show slightly lower H₂O at rims compared to cores, which could indicate either a limited extent of H₂O loss during eruption, or H₂O decrease due to subsolidus cooling (Chin et al., 2016). In summary, there is no evidence that H₂O was added to mineral grains during kimberlite eruption. While H₂O could have been lost from mineral grains during eruption, the observation that inter-mineral H₂O contents largely reflect equilibrium D values suggests that eruption-induced loss was also probably minimal (since kimberlites erupt on extremely rapid timescales). However, H₂O “loss” – or, alternatively, as we discuss later – decreased H₂O solubility within an approximate equilibrium state of subsolidus cooling, indicates that our measured H₂O contents are minimum bounds.

5.2 Reconstructed bulk rock H_2O and calculated melt H_2O

In the previous section, we established that inter-mineral H_2O ratios in the State Line xenoliths fall within range of experimental mineral/melt D values. This observation justifies our approach, described below, of calculating equilibrium melt H_2O contents that could have last been in equilibrium with our xenoliths.

Before further discussing recalculated bulk rock H_2O and hypothetical melt compositions, it is important to revisit the cooling history of the State Line lower crustal xenoliths and the impact on measured H_2O contents. Petrographic and textural observations of the xenoliths point to subsolidus cooling, such as the abundance of garnet-clinopyroxene coronas interpreted to have formed at the expense of orthopyroxene and plagioclase (Farmer et al., 2005). Although coronas could result from increasing temperature and pressure (e.g. prograde metamorphism from medium to high-grade granulites), they have also been proposed to form via isobaric cooling (due to the slope of the spinel-garnet transition, **Fig. 8**; Kushiro and Yoder (1966)) or cooling with increasing pressure (Chin et al., 2012; Saltzer et al., 2001). We consider that State Line xenoliths experienced subsolidus cooling following lower crustal stabilization sometime in the Proterozoic (as previously proposed by Farmer et al. (2005)). If this is the case, H_2O contents measured in nominally anhydrous minerals likely represent minimum bounds, due to the lowering of H_2O solubility with decreasing temperature (cf. Zhao et al. (2004)). Note that the effect of temperature on H_2O solubility is well-constrained for olivine, but not for pyroxenes. Unlike olivine, some mechanisms of water incorporation in pyroxene are thought to be coupled to slow-diffusing cations, such as the exchange $Al^{3+} + H^+ = Si^{4+}$; Keppler and Bolfan-Casanova (2006). Thus, it might be expected that the cooling effect on H_2O solubility may not be as extreme as that in olivine. Future experimental work may shed new insights into H_2O solubility in minerals other than olivine. What matters for the present study is that calculated melt H_2O contents using our measured H_2O contents and D values are likely to be minimum bounds due to cooling.

If we consider that subsolidus cooling could have decreased the absolute concentrations of H_2O in NAMs, but that cooling occurred such that inter-mineral H_2O ratios continued to reflect ambient equilibrium conditions (as observed in inter-mineral H_2O ratios), we can reconstruct bulk rock H_2O using maximum observed mineral H_2O

contents as a way to “see past” the effect of cooling (cf. Chin et al. (2016)). Although the spread of H₂O contents within individual mineral grains is low (i.e., negligible core-rim zoning), within individual xenoliths the H₂O contents of the grain population can be variable (**Table 2**), but does not vary more than ~30% (RSD) within a given xenolith. For instance, clinopyroxene H₂O varies from a minimum of 476 ppm to a maximum of 1225 ppm in SD2-LC110; out of a population of 9 clinopyroxene grains, only two grains had H₂O above the average value of 637 ppm for the whole population. Within those two grains with high H₂O, multiple spots yielded reproducible results (within 15%). We also note that because of the time-resolved and *in situ* context of the SIMS measurements, any measurements that could have been contaminated by fluid inclusions or other impurities are easily resolved and can be removed during data reduction. Thus, we are confident that any grains with H₂O above the average value for a given xenolith are likely to be real, and still reflect minimum bounds on the naturally preserved H₂O contents. Using maximum observed H₂O contents and mineral modes, reconstructed bulk rock H₂O range from 82 ppm (SH-E1) to 651 ppm (SD2-LC110). In comparison, reconstructed bulk rock H₂O using average mineral H₂O values give a range from 58 to 406 ppm.

Next, we calculate H₂O contents of melts last in equilibrium with the bulk reconstructed xenolith H₂O contents (**Table 2**). To do so, we first determine a bulk D_{H₂O} value for each xenolith using experimental D values and mineral modes, which is then used to calculate C_{H₂O melt}. For garnet-bearing xenoliths, we determined melt water contents ranging from 0.8 wt.% (SH-E1) to 5.5 wt.% (SD2-LC110) (using average mineral H₂O; if maximum mineral H₂O are used, calculated melt H₂O will be higher). We calculated melt water content of 2.2 wt% for one garnet-free xenolith (SD2-LC75). Calculated melt H₂O contents increase with decreasing clinopyroxene Mg# and decreasing modal garnet and clinopyroxene. The calculated melt H₂O is noted next to each xenolith in **Fig. 6a**.

5.3 A cumulate, arclogite origin for the State Line lower crustal suite

Previous studies on the State Line lower crustal granulite xenoliths lack clarity on the origin and tectonic setting of the protoliths. While all agreed the protolith had to be related to some form of basaltic magmatism, three competing hypotheses as to the magmatic process responsible were proposed by Lester and Farmer (1998) and Farmer et

al. (2005): cumulates, restites, or *in situ* crystallized basaltic melt. Furthermore, the tectonic setting of the protoliths (e.g., subduction zone, oceanic ridge, or intraplate rift) is unclear, owing to ambiguity in interpreting bulk rock trace element data, particularly highly incompatible elements (Sr, Rb, K), that may have been compromised by kimberlite contamination.

Using our new data on H₂O concentrations in NAMs in the State Line xenoliths, we provide new insights into the nature of the protoliths and their tectonic setting. A key finding from our analysis of the H₂O data is that the *minimum* water content of the melt last in equilibrium with the most primitive xenolith is already quite hydrous (~1 wt.% H₂O) compared to typical primitive MORB (~0.1 wt%; Sobolev and Chaussidon (1996)). Calculated melt water contents increase with decreasing Mg# (**Fig. 6b**), consistent with a fractional crystallization trend wherein the xenoliths could represent (now metamorphosed) crystal cumulates. While a similar trend might also be predicted for a restite (partial melting) trend, we might expect mineral and bulk rock H₂O contents to be even lower than observed if significant partial melting occurred, which should effectively remove all or most of the water. It is also unlikely that the State Line xenoliths represent “frozen in” basaltic melts trapped at depth, if we assume that their protoliths were MORB-like in terms of H₂O content, as has been proposed for arc basement in the Colorado Province (Cavosie & Selverstone, 2003). Moreover, if MORB-like melts crystallized at initially shallow pressures and then cooled during thickening of a boundary layer, we should expect bulk rock H₂O contents less than or equal to typical water contents of primitive MORB melts, which are at least 10x lower than our bulk rock H₂O. Thus, we propose that the State Line lower crustal xenoliths represent cumulates from a hydrous melt.

Comparison of the State Line lower crustal xenoliths with other deep crustal cumulates also supports an origin by crystal fractionation from hydrous magmas. Although the overall major element composition of most of the xenoliths would place them within the field of typical MORB olivine tholeiite (Bradley & McCallum, 1984; Lester & Farmer, 1998), from **Fig. 7** it is apparent that over 50% of the xenoliths have whole-rock Mg#'s greater than average MORB. In addition, the CaO and SiO₂ content of most State Line lower crustal xenoliths are lower than average MORB (**Fig. 7b, c**). FeO_T

contents of the xenoliths also extend to higher values than average MORB (**Fig. 7e**). The State Line lower crustal xenoliths also generally do not fall within the field of global MORB cumulates. Although the mean Mg# of MORB cumulates (71; Chin et al. (2018)) is higher than the mean Mg# of the State Line xenoliths (60), the major element trends of the State Line xenoliths differ from MORB cumulates. For instance, the State Line xenoliths do not show Al_2O_3 enrichment at high Mg# signifying cotectic olivine + plagioclase crystallization characteristic of MORB cumulates. This is manifested modally by the absence of olivine in the State Line xenoliths. The State Line xenoliths also plot in regions distinct from MORB cumulates in SiO_2 vs. Mg# and Na_2O vs. Mg# plots (**Fig. 7c, d**).

The State Line xenoliths do overlap compositionally with the Sierran and Arizona arclogite xenolith field. Arclogites are distinct from eclogites, the former representing garnet and pyroxene-rich cumulates from primitive, hydrous arc magmas (Lee & Anderson, 2015), whereas the latter are metamorphosed equivalents of basalt. The mean Mg# of 60 for State Line xenoliths is similar to the range reported for low-MgO garnet pyroxenites from the Sierra Nevada (Lee et al., 2006) and also the mean of ~62 for island and continental arcs (Chin et al., 2018). Furthermore, the State Line xenoliths have similar Al_2O_3 at a given Mg# range as low-MgO arclogites (**Fig. 7a**); their FeOT contents also extend to elevated values similar to arclogites (**Fig. 7e**) and in contrast to Fe-poor MORB cumulates. CaO contents are overall similar, but slightly lower, than arclogite xenoliths (**Fig. 7b**). Although the SiO_2 content shows a wide range from 43 to 52 wt.%, approximately half of the State Line xenoliths have SiO_2 overlapping with Sierran and Arizona arclogites.

We compare clinopyroxene compositions from the State Line xenoliths to other published data on deep lithospheric clinopyroxenes. These include clinopyroxenes from global peridotite and eclogite xenoliths (see **Figure 5 caption** for references), arclogites from Mesozoic arcs in Western North America (Erdman et al., 2016; Lee et al., 2006), intraplate clinopyroxenite cumulates from Tanzania (Chin, 2018), and granulite xenoliths from the lower crust of the North China Craton (Yang et al., 2008). The State Line clinopyroxenes clearly fall off the high-pressure mantle array represented by garnet peridotite and eclogite (*sensu stricto*) xenoliths; the former are confined to a narrow

range of Na₂O and CaO contents, while the latter trend towards high Na₂O and low CaO (Fig. 5a, b). Clinopyroxene from granulite xenoliths from N. China are also distinct from the State Line clinopyroxenes. This could be attributed to the lower modal abundance of garnet in the N. China granulites – most of these granulites are garnet-free, and those that contain garnet have it in abundances of 25% or less (Yang et al., 2008), in contrast to garnet-bearing State Line xenoliths, which have >25% garnet. Again, similar to bulk rock trends, State Line clinopyroxenes overlap most with clinopyroxenes from low-MgO garnet pyroxenites from arclogite xenoliths. Similarities between State Line and low-MgO arclogite clinopyroxenes are most clear in Na₂O vs. MgO, CaO vs. MgO, and Al₂O₃ vs. MgO (Fig. 5a, b, c). TiO₂ contents are overall higher than arclogite clinopyroxene, but the steep vertical trend in the TiO₂ vs. MgO plot is similar to steep trends observed in other cumulate-type rocks (e.g. N. China and Tanzania). One possibility for the discrepancy in TiO₂ between State Line and arclogite clinopyroxene is that in many arclogites, rutile was reported as an exsolution product from garnet and clinopyroxene (Erdman et al., 2016; Lee et al., 2006).

5.4 Deep, hydrous fractional crystallization

Based on the discussion above, H₂O systematics, whole rock, and clinopyroxene compositional data all suggest that the State Line lower crustal xenoliths could represent crystal cumulates from primitive, hydrous magmas. Crystallization experiments of hydrous basaltic andesites at deep crustal conditions (~1 GPa) produced cumulates with variable amounts of garnet, plagioclase, hornblende, clinopyroxene, and orthopyroxene (Muntener & Ulmer, 2006), broadly similar (with the exception of hornblende) to our xenoliths. The prevalence of hornblende in the experiments is probably due to the relatively high melt H₂O contents in the starting material (4 – 8 wt.%). Hornblende may have once been present in our xenoliths prior to final equilibration in the granulite facies, and hornblende is present in small amounts in some xenoliths (Farmer et al., 2005).

Primitive melt inclusions from subduction zones worldwide show a well-defined average H₂O content of 3.9 wt.% ± 0.4 (Plank et al., 2013). 5.5 and 4.6 wt. % H₂O in the melt was calculated for garnet-bearing xenoliths SD2-LC110 and SD2-LC71, respectively (Table 2; Fig. 6), which both have clinopyroxene Mg#s ~72 – 75 and high modal proportions of garnet and clinopyroxene. These values are similar to those found

in primitive melt inclusions; interestingly, melt inclusions hosted in the most primitive olivines ($>Fo_{86}$) seem to have higher H_2O than those in $<Fo_{85}$ olivine (Plank et al., 2013), with some values as high as ~ 6 wt.% H_2O (Fig. 1 in Plank et al. (2013)). Experimental petrology also indicates that basaltic systems at high pressures experience a widened stability field for clinopyroxene (Kushiro & Yoder, 1969), and with more andesitic compositions, garnet and clinopyroxene are expected to be the first liquidus phases (Alonso-Perez et al., 2009). Thus, the overall modal mineralogy of xenoliths SD2-LC110 and SD2-LC71 resemble experimental cumulates of crystal fractionation of hydrous andesite. Below, we discuss the similarity in calculated equilibrium melt H_2O with the ~ 4 wt.% H_2O average observed in arc melt inclusions.

While in a broad sense, we interpret the State Line lower crustal xenoliths to represent cumulates from primitive, hydrous melts, it is unclear whether all the xenoliths in the suite represent one crystal line of descent from a single parent magma, or “instantaneous” cumulates from various (but petrologically similar) magmas. Due to the nature of xenolith sampling, it is probably impossible to answer this question. Thus, it is possible that the ~ 5 wt.% melt H_2O we calculated for garnet-bearing xenoliths SD2LC-110 and SD2LC-71 (**Table 2**) could reflect a “snapshot” of part of the crystal line of descent, and so melt H_2O would be expected to vary where a given cumulate is along that line of descent. One way to “see through” to the H_2O content of the parental magma is to consider the most primitive (highest Mg#) cumulates, as these cumulates would have fractionated out early along the magmatic differentiation path. If we consider the most primitive xenolith in our suite, SH-E1 (highest clinopyroxene Mg#) as one of the earliest crystal cumulates to fractionate from a hydrous basaltic melt, the observed mineral modes match the near bi-mineralic assemblages of early experimental cumulates (Alonso-Perez et al., 2009) as well as natural cumulate arclogites (Lee et al., 2006). Using a simple Rayleigh fractional crystallization model, assuming we start with 1 wt.% H_2O in the melt (although we calculated 0.8 wt.% H_2O in equilibrium SH-E1, we use 1 wt.% for simplicity; using 0.8 wt.% does not change the final result significantly), a fractionating assemblage of clinopyroxene and garnet in ratios ranging from 50:50 to 25:75, and a $D_{bulk} = 0.004$, and allow this melt to crystallize to $F = 0.4$, results in melt H_2O of ~ 4 wt.%, similar to the global primitive melt inclusion average. Thus, fractional crystallization of

a melt with ~1 wt.% H₂O will not only produce garnet-clinopyroxene cumulates similar to those observed in our samples, but can also evolve melts at ~50% crystallization with H₂O contents that agree with primitive melt inclusions. We further note that more mafic melts have lower critical melt fractions (Paterson et al., 1998), and so melt extraction will occur at lower crystallinities and generally be more efficient compared to more silicic melts. This would be facilitated even more with hydrous melts, owing to the high incompatibility of water – early melts can have high starting H₂O, and with increasing crystal fractionation, will become even more enriched in H₂O. This could be one way that deep crustal fractional crystallization sets the stage for further magmatic evolution in the middle crust, where amphibole can become stable at high melt H₂O contents (Davidson et al., 2007).

5.5 Geologic & tectonic implications

Though now metamorphosed into the granulite facies, we propose that the State Line lower crustal xenoliths were originally crystal cumulates from hydrous melts. The presence of both garnet-free, plagioclase-bearing xenoliths and garnet and clinopyroxene-rich xenoliths could represent two magmatic lineages with lower and higher melt H₂O contents, respectively. One geologic scenario that could explain this dichotomy is the following. The Yavapai arc terrane is thought to represent products of oceanic island arc magmatism that accreted onto the North American continent during the Yavapai Orogeny (1.8 – 1.7 Ga). During oceanic island arc magmatism, the lithosphere is generally under extension and melting degrees can be moderate to high, producing primary melts at shallower pressures and with lower melt H₂O (**1 in Fig. 8**). Such melts might fall more along a tholeiitic trend and would produce cumulates comprised mostly of pyroxene and plagioclase (gabbros).

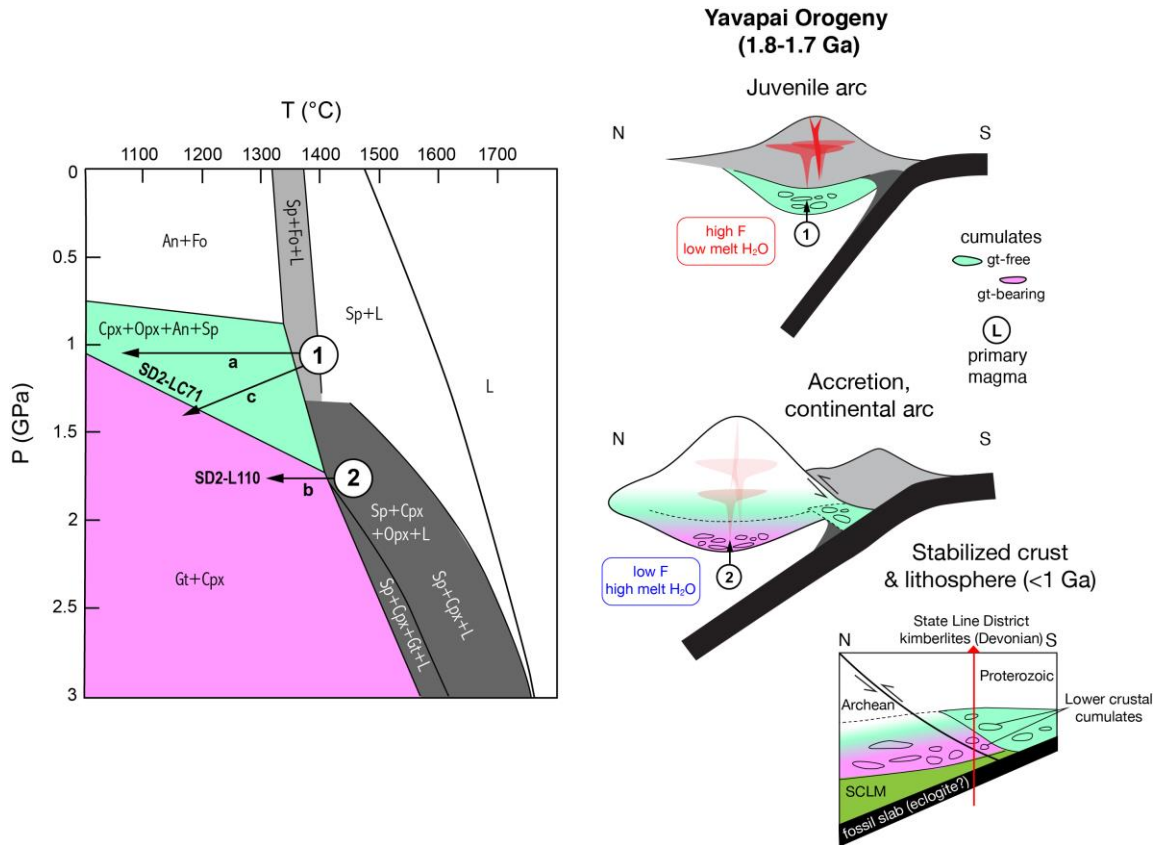


Fig. 8. Petrologic & geologic interpretation. Phase diagram for a bulk composition of 1:1 molecular anorthite and forsterite, from Kushiro and Yoder (1966). 1 and 2 represent hypothetical protoliths of SD2-LC71 and SD2-L110, respectively. 1 is a magma with cpx, opx, spinel, \pm olivine on its liquidus; upon cooling it would crystallize cumulates with the mineralogy cpx+opx+plagioclase+spinel (green field – gabbros). 2 is a slightly higher pressure magma without olivine on the liquidus; upon cooling it would crystallize garnet+cpx cumulates. Paths a, b, and c represent possible subsolidus P-T paths. See text for details. Right: Proposed tectonic model associated with the Proterozoic Yavapai Orogeny. Block diagram after Eggler et al. (1988) showing architecture of the crust and lithosphere following accretion and stabilization.

The Yavapai arc system may have evolved to a continental arc as the terrane sutured onto North America; Proterozoic calc-alkaline plutons in the vicinity of the State Line District may be evidence of this (Karlstrom & Houston, 1984). Cavosie and Selverstone (2003) proposed that the ~ 1.7 Ga arc magmatism of the Colorado province may have been built initially on oceanic crust, which originated either as a ridge-transform intersection or a backarc spreading center, and then was subsequently entrapped during accretion of the Yavapai terrane onto the Wyoming Craton. During this transition, the crust presumably thickened, resulting in progressively deeper melt

generation depths and thus lower degrees of melting (Plank & Langmuir, 1988), and hence higher initial melt H₂O (Chin et al., 2018). Such higher-H₂O and higher pressure melts would crystallize liquidus garnet and clinopyroxene as early cumulates (**2 in Fig. 8**), represented now in the State Line xenoliths as the garnet-rich granulites. The scenario proposed above could also explain the transitional nature of the State Line lower crustal xenolith suite, which shows gradation from gabbros (tholeiitic trend) to more garnet and clinopyroxene-rich assemblages (calc-alkaline trend). Following cooling into the granulite facies, the Proterozoic State Line lower crust stabilized and was subsequently tectonically juxtaposed over Archean lithosphere (Eggler et al., 1988), and then sampled by kimberlites in the Devonian (**Fig. 8**).

The occurrence of abundant garnet-pyroxene coronas is also consistent with two, or possibly more, distinct arc magma lineages that subsequently experienced P-T paths governed by where they started along the solidus in **Fig. 8**. Analysis of the phase boundaries in **Fig. 8** shows that near-solidus cumulates of a low pressure, tholeiitic melt 1 in **Fig. 8** would have to cool to a large extent to enter the garnet stability field due to the slope of the spinel-garnet transition (path a). Note that garnet formation solely due to isobaric cooling of plagioclase-rich protoliths, such as composition 1 in **Fig. 8**, is kinetically inefficient (Chapman et al., 2017). This could explain the substantial population of plagioclase-bearing granulites in the State Line suite. By contrast, near-solidus cumulates of a deeper, presumably more calc-alkaline and hydrous, melt 2 in **Fig. 8** would already have spinel, clinopyroxene ± orthopyroxene, and garnet as liquidus phases, and a smaller extent of cooling would immediately precipitate garnet and clinopyroxene as early cumulate minerals, like xenolith SD2-L110 (path b). Alternatively, a protolith starting at 1 in **Fig. 8** could undergo an increase in pressure while cooling (path c) (Chin et al., 2016), which would pivot more quickly to the garnet stability field due to the slope of the garnet-in boundary, allowing coronas to form without a large amount of cooling. This could be the case for SD2-LC71 and the “mixed” granulites that contain various proportions of plagioclase but abundant garnet+cpx coronas.

Our EBSD data also suggest a history more complex than simple isobaric cooling for the corona-bearing xenoliths. Microstructural observations in SD2-LC71 show

abundant deformation twins in plagioclase porphyroclasts, and large clinopyroxene grains more deformed than fine-grained clinopyroxene inside garnet coronas (**Fig. 2g, Fig. 4**), suggesting that delicate corona structures formed after an earlier ductile deformation. Such a two-stage deformation history could be explained by a thickening + cooling path. We conclude that isobaric cooling alone – a P-T path typically associated with plume underplating – is likely not sufficient to account for the high modal garnet (>25 %) and clinopyroxene (>30%) in many of the State Line xenoliths. Together with H₂O contents in NAMs consistent with an igneous cumulate heritage and microstructural evidence of a complex deformation history encapsulated between ~1.8 and ~400 Ma, we therefore propose that the State Line granulites represent deep remnants of continental crust formed in an evolving arc setting in the Proterozoic.

Finally, while garnet-rich arc cumulates are critical for facilitating delamination or convective removal of thickened arc roots (Lee & Anderson, 2015), it should not go unnoticed that plagioclase-bearing cumulates are also an important constituent of igneous arc lithosphere. The origin of these gabbroic cumulates is less clear, since they could have formed either in juvenile arcs that were subsequently accreted, or perhaps at oceanic ridges. The buoyancy of gabbroic cumulates relative to garnet-bearing cumulates may allow them to survive capture and suturing, thereby providing a buoyant “life raft” onto which subsequent calc-alkaline continental arc magmatism may grow upon. In the Sierra Nevada Batholith, archetype of a continental arc, Ducea and Saleeby (1996) showed that gabbros, cumulate gabbros, and plagioclase granulites are nearly as abundant as garnet clinopyroxenites within the well-studied Sierra Nevada deep lithospheric xenolith suite. They further note that compositionally, the gabbroic cumulates and granulites overlap in terms of major element bulk composition with garnet clinopyroxenites, indicating a similar gradational spectrum observed in the State Line lower crust.

Parallels between the State Line xenoliths with Phanerozoic arclogites suggests that arcs could have operated in a similar manner in the Proterozoic. Our data on the H₂O content of granulite-facies rocks – typically thought to be “bone dry” – indicates that such rocks can contain significant H₂O: up to ~1000 ppm in clinopyroxene and bulk H₂O ranging ~400 to ~650 ppm. Such values are at least a factor of two higher than maximum estimates for the upper mantle, the layer directly beneath the lower crust. Moreover, our

measured H₂O contents are likely to be minimum bounds due to decreased solubility during cooling. This implies that lower crust formed in Proterozoic arcs could have been just as hydrous, or even more hydrous than what is observed today.

6 Conclusions

We investigated the water contents of nominally anhydrous minerals, as well as modal mineralogy and rock microstructure, in lower crustal xenoliths from the State Line kimberlite district in northern Colorado, USA. Average water contents for minerals range from 75 to 760 ppm, 233 to 410 ppm, and 42 to 139 ppm for clinopyroxene, orthopyroxene, and garnet, respectively. Despite subsolidus cooling, inter-mineral water partitioning largely reflects equilibrium D values, indicating closed system conditions. Importantly, the coherence between measured inter-mineral partitioning and D values allows us to constrain minimum bounds on water contents of melts last in equilibrium with the xenoliths. Calculated melt water contents range from ~1 to ~5 wt.%. Together with the high garnet and clinopyroxene mode in many of the xenoliths and their overall resemblance to arclogite xenoliths from well-known arcs, we interpret the State Line xenoliths to have originally been igneous cumulates from moderate to high pressure, hydrous magmas associated with arc magmatism during Proterozoic accretion of North America.

Acknowledgments, Samples, and Data

The authors are grateful for constructive reviews from XXX and to Editor XXX for handling the manuscript. EJC thanks Joe Boesenberg for assistance on the Brown University EPMA and Lonnie Hufford for EBSD assistance. EJC and STC thank Yunbin Guan for help on SIMS. This work was supported by grants from the National Science Foundation to EJC (NSF EAR 1719208 and NSF EAR 1855407). The authors declare no financial interests that could be perceived as being a conflict of interest. Data archiving for this research is currently underway and will be located at earthchem.org.

References

- Alonso-Perez, R., Muntener, O., & Ulmer, P. (2009). Igneous garnet and amphibole fractionation in the roots of island arcs: experimental constraints on andesitic liquids. *Contributions to Mineralogy and Petrology*, 157(4), 541-558. doi:10.1007/s00410-008-0351-8
- Arndt, N. T. (2013). The formation and evolution of the continental crust. *Geochemical Perspectives*, 2(3), 405-405.

- Ater, P., Eggler, D., & McCallum, M. (1984). Petrology and geochemistry of mantle eclogite xenoliths from Colorado-Wyoming kimberlites: recycled ocean crust? *Developments in Petrology* (Vol. 11, pp. 309-318): Elsevier.
- Aubaud, C., Hauri, E. H., & Hirschmann, M. M. (2004). Hydrogen partition coefficients between nominally anhydrous minerals and basaltic melts. *Geophysical Research Letters*, 31(20).
- Aubaud, C., Withers, A. C., Hirschmann, M. M., Guan, Y., Leshin, L. A., Mackwell, S. J., & Bell, D. R. (2007). Intercalibration of FTIR and SIMS for hydrogen measurements in glasses and nominally anhydrous minerals. *American Mineralogist*, 92(5-6), 811-828.
- Avé Lallemant, H. G. (1969). Structural and petrofabric analysis of an “alpine-type” peridotite: the lherzolite of the French Pyrenees. *Leidse Geologische Mededelingen*, 42(1), 1-57.
- Beard, B., Fraracci, K. N., Clayton, R. A., Mayeda, T. K., Snyder, G., Sobolev, N., & Taylor, L. (1996). Petrography and geochemistry of eclogites from the Mir kimberlite, Yakutia, Russia. *Contributions to Mineralogy and Petrology*, 125(4), 293-310.
- Bickford, M., Van, W., & Zietz, I. (1986). Proterozoic history of the midcontinent region of North America. *Geology*, 14(6), 492-496.
- Boyd, F. R., & Mertzman, S. A. (1987). Composition and structure of the Kaapvaal lithosphere, Southern Africa. In B. O. Mysen (Ed.), *Magmatic Processes: Physicochemical Principles* (Vol. 1, pp. 13-25): The Geochemical Society.
- Bradley, S. D., & McCallum, M. (1984). Granulite facies and related xenoliths from Colorado-Wyoming kimberlite *Developments in Petrology* (Vol. 11, pp. 205-217): Elsevier.
- Cavosie, A., & Selverstone, J. (2003). Early Proterozoic oceanic crust in the northern Colorado Front Range: Implications for crustal growth and initiation of basement faults. *Tectonics*, 22(2).
- Chapman, T., Clarke, G. L., Piazzolo, S., & Daczko, N. R. (2017). Evaluating the importance of metamorphism in the foundering of continental crust. *Scientific reports*, 7(1), 1-12.
- Chin, E. J. (2018). Deep crustal cumulates reflect patterns of continental rift volcanism beneath Tanzania. *Contributions to Mineralogy and Petrology*, 173(10), 85.
- Chin, E. J., Lee, C.-T. A., Luffi, P., & Tice, M. (2012). Deep Lithospheric Thickening and Refertilization beneath Continental Arcs: Case Study of the P, T and Compositional Evolution of Peridotite Xenoliths from the Sierra Nevada, California. *Journal of Petrology*, 53(3), 477-511. doi:10.1093/petrology/egr069
- Chin, E. J., Shimizu, K., Bybee, G. M., & Erdman, M. E. (2018). On the development of the calc-alkaline and tholeiitic magma series: A deep crustal cumulate perspective. *Earth and Planetary Science Letters*, 482, 277-287. doi:https://doi.org/10.1016/j.epsl.2017.11.016
- Chin, E. J., Soustelle, V., Hirth, G., Saal, A., Kruckenberg, S. C., & Eiler, J. (2016). Microstructural and geochemical constraints on the evolution of deep arc lithosphere. *Geochemistry, Geophysics, Geosystems*, n/a-n/a. doi:10.1002/2015GC006156
- Collins, W. J., Murphy, J. B., Johnson, T. E., & Huang, H.-Q. (2020). Critical role of water in the formation of continental crust. *Nature Geoscience*, 1-8.
- Davidson, J., Turner, S., Handley, H., Macpherson, C., & Dosseto, A. (2007). Amphibole “sponge” in arc crust? *Geology*, 35(9), 787-790.
- Dickinson, W. R., & Snyder, W. S. (1978). Plate tectonics of the Laramide orogeny. In V. Matthews (Ed.), *Laramide folding associated with basement block faulting in the Western United States*, *Geological Society of America Memoir 151* (pp. 355-366).
- Ducea, M. N., & Saleeby, J. B. (1996). Buoyancy sources for a large, unrooted mountain range, the Sierra Nevada, California: Evidence from xenolith thermobarometry. *J. Geophys. Res.*, 101(B4), 8229-8244. doi:10.1029/95jb03452
- Eggler, D., Meen, J., Welt, F., Dudas, F. O., Furlong, K., McCallum, M., & Carlson, R. (1988). Tectonomagmatism of the Wyoming province. *Colorado School of Mines Quarterly*, 83(2), 25-40.
- Eggler, D. H., McCallum, M., & Kirkley, M. (1987). Kimberlite-transported nodules from Colorado-Wyoming. *A record of enrichment of shallow portions of an infertile lithosphere: Geological Society of America Special Paper*, 215, 77-90.
- Ehrenberg, S. N. (1982). Petrogenesis of garnet lherzolite and megacrystalline nodules from the Thumb, Navajo volcanic field. *Journal of Petrology*, 23(4), 507-547.
- Erdman, M. E., Lee, C.-T. A., Levander, A., & Jiang, H. (2016). Role of arc magmatism and lower crustal foundering in controlling elevation history of the Nevadaplano and Colorado Plateau: A case study

- of pyroxenitic lower crust from central Arizona, USA. *Earth and Planetary Science Letters*, 439, 48-57.
- Farmer, G. L., Bowring, S. A., Williams, M. L., Christensen, N. I., Matzel, J. P., & Stevens, L. (2005). Contrasting lower crustal evolution across an Archean-Proterozoic suture: Physical, chemical and geochronologic studies of lower crustal xenoliths in southern Wyoming and northern Colorado. *Washington DC American Geophysical Union Geophysical Monograph Series*, 154, 139-162.
- Farmer, G. L., Fritz, D. E., & Glazner, A. F. (2020). Identifying Metasomatized Continental Lithospheric Mantle Involvement in Cenozoic Magmatism From Ta/Th Values, Southwestern North America. *Geochemistry, Geophysics, Geosystems*, 21(5), e2019GC008499. doi:10.1029/2019gc008499
- Franz, L., Brey, G. P., & Okrusch, M. (1996). Steady state geotherm, thermal disturbances, and tectonic development of the lower lithosphere underneath the Gibeon Kimberlite Province, Namibia. *Contributions to Mineralogy and Petrology*, 126(1-2), 181-198.
- Fung, A. T., & Haggerty, S. E. (1995). Petrography and mineral compositions of eclogites from the Koidu Kimberlite Complex, Sierra Leone. *Journal of Geophysical Research: Solid Earth*, 100(B10), 20451-20473.
- Hauri, E. H., Gaetani, G. A., & Green, T. H. (2006). Partitioning of water during melting of the Earth's upper mantle at H₂O-undersaturated conditions. *Earth and Planetary Science Letters*, 248(3), 715-734.
- Hervig, R. L., Smith, J. V., & Dawson, J. B. (1986). Lherzolite xenoliths in kimberlites and basalts: petrogenetic and crystallochemical significance of some minor and trace elements in olivine, pyroxenes, garnet and spinel. *Earth and Environmental Science Transactions of the Royal Society of Edinburgh*, 77(03), 181-201. doi:10.1017/S026359330001083X
- Hills, D. V., & Haggerty, S. E. (1989). Petrochemistry of eclogites from the Koidu kimberlite complex, Sierra Leone. *Contributions to Mineralogy and Petrology*, 103(4), 397-422.
- Hirth, G., & Kohlstedt, D. L. (1995). Experimental constraints on the dynamics of the partially molten upper mantle: 2. Deformation in the dislocation creep regime. *Journal of Geophysical Research: Solid Earth* (1978-), 100(B8), 15441-15449.
- Humphreys, E., Hessler, E., Dueker, K., Farmer, G., Erslev, E., & Atwater, T. (2003). How Laramide-Age Hydration of North American Lithosphere by the Farallon Slab Controlled Subsequent Activity in the Western United States. *International Geology Review*, 45(7), 575 - 595.
- Jones, C. H., Mahan, K. H., Butcher, L. A., Levandowski, W. B., & Farmer, G. L. (2015). Continental uplift through crustal hydration. *Geology*, 43(4), 355-358.
- Karlstrom, K., & Houston, R. (1984). The Cheyenne belt: Analysis of a Proterozoic suture in southern Wyoming. *Precambrian Research*, 25(4), 415-446.
- Katayama, I., Nakashima, S., & Yurimoto, H. (2006). Water content in natural eclogite and implication for water transport into the deep upper mantle. *Lithos*, 86(3-4), 245-259.
- Keppler, H., & Bolfan-Casanova, N. (2006). Thermodynamics of water solubility and partitioning. *Reviews in Mineralogy and Geochemistry*, 62(1), 193-230.
- Kushiro, I., & Yoder, H. S. (1969). Melting of forsterite and enstatite at high pressures under hydrous conditions. *Carnegie Inst Washington Yearb*, 67, 153-161.
- Kushiro, I., & Yoder Jr, H. (1966). Anorthite—forsterite and anorthite—enstatite reactions and their bearing on the basalt—eclogite transformation. *Journal of Petrology*, 7(3), 337-362.
- Lange, R. A., Carmichael, I. S., & Hall, C. M. (2000). 40Ar/39Ar chronology of the Leucite Hills, Wyoming: Eruption rates, erosion rates, and an evolving temperature structure of the underlying mantle. *Earth and Planetary Science Letters*, 174(3-4), 329-340.
- Lee, C.-T., & Anderson, D. (2015). Continental crust formation at arcs, the arclogite “delamination” cycle, and one origin for fertile melting anomalies in the mantle. *Science Bulletin*, 1-16. doi:10.1007/s11434-015-0828-6
- Lee, C.-T. A., & Anderson, D. L. (2015). Continental crust formation at arcs, the arclogite “delamination” cycle, and one origin for fertile melting anomalies in the mantle. *Science Bulletin*, 60(13), 1141-1156.
- Lee, C.-T. A., Cheng, X., & Horodyskyj, U. (2006). The development and refinement of continental arcs by primary basaltic magmatism, garnet pyroxenite accumulation, basaltic recharge and delamination: insights from the Sierra Nevada. *Contributions to Mineralogy and Petrology*, 151, 222-242. doi:10.1007/s00410-005-0056-1

- Lester, A., & Farmer, G. L. (1998). Lower crustal and upper mantle xenoliths along the Cheyenne belt and vicinity. *Rocky Mountain Geology*, 33(2), 293-304.
- Li, Z.-X. A., Lee, C.-T. A., Peslier, A. H., Lenardic, A., & Mackwell, S. J. (2008). Water contents in mantle xenoliths from the Colorado Plateau and vicinity: Implications for the mantle rheology and hydration-induced thinning of continental lithosphere. *Journal of Geophysical Research: Solid Earth*, 113(B9), n/a-n/a. doi:10.1029/2007jb005540
- Lin, Y., Hui, H., Li, Y., Xu, Y., & Van Westrenen, W. (2019). A lunar hygrometer based on plagioclase-melt partitioning of water. *Geochemical Perspectives Letters*, 10, 14-19.
- Liu, J., Xia, Q.-K., Kuritani, T., Hanski, E., & Yu, H.-R. (2017). Mantle hydration and the role of water in the generation of large igneous provinces. *Nature Communications*, 8(1), 1-8.
- McLelland, J. M., & Whitney, P. R. (1980). A generalized garnet-forming reaction for metagneous rocks in the Adirondacks. *Contributions to Mineralogy and Petrology*, 72(2), 111-122.
- Mosenfelder, J. L., Le Voyer, M., Rossman, G. R., Guan, Y., Bell, D. R., Asimow, P. D., & Eiler, J. M. (2011). Analysis of hydrogen in olivine by SIMS: Evaluation of standards and protocol. *American Mineralogist*, 96(11-12), 1725-1741.
- Mosenfelder, J. L., & Rossman, G. R. (2013a). Analysis of hydrogen and fluorine in pyroxenes: I. Orthopyroxene. *American Mineralogist*, 98(5-6), 1026-1041.
- Mosenfelder, J. L., & Rossman, G. R. (2013b). Analysis of hydrogen and fluorine in pyroxenes: II. Clinopyroxene. *American Mineralogist*, 98(5-6), 1042-1054.
- Muntener, O., & Ulmer, P. (2006). Experimentally derived high-pressure cumulates from hydrous arc magmas and consequences for the seismic velocity structure of lower arc crust. *Geophysical Research Letters*, 33(21), L21308. doi:10.1029/2006gl027629
- Paterson, S. R., Fowler Jr, T. K., Schmidt, K. L., Yoshinobu, A. S., Yuan, E. S., & Miller, R. B. (1998). Interpreting magmatic fabric patterns in plutons. *Lithos*, 44(1-2), 53-82.
- Plank, T., Kelley, K. A., Zimmer, M. M., Hauri, E. H., & Wallace, P. J. (2013). Why do mafic arc magmas contain ~4wt% water on average? *Earth and Planetary Science Letters*, 364, 168-179.
- Plank, T., & Langmuir, C. H. (1988). An evaluation of the global variations in the major element chemistry of arc basalts. *Earth and Planetary Science Letters*, 90(4), 349-370.
- Rehfeldt, T., Jacob, D. E., Carlson, R. W., & Foley, S. F. (2007). Fe-rich dunite xenoliths from South African kimberlites: cumulates from Karoo flood basalts. *Journal of Petrology*, 48(7), 1387-1409.
- Reid, A. M., Donaldson, C., Brown, R., Ridley, W., & Dawson, J. (1975). Mineral chemistry of peridotite xenoliths from the Lashaine volcano, Tanzania *Physics and Chemistry of the Earth* (pp. 525-543): Elsevier.
- Rudnick, R. L. (1995). Making continental crust. *Nature*, 378(6557), 571-578.
- Saltzer, R. L., Chatterjee, N., & Grove, T. L. (2001). The Spatial Distribution of Garnets and Pyroxenes in Mantle Peridotites: Pressure-Temperature History of Peridotites from the Kaapvaal Craton. *Journal of Petrology*, 42(12), 2215-2229. doi:10.1093/petrology/42.12.2215
- Sobolev, A. V., & Chaussidon, M. (1996). H₂O concentrations in primary melts from supra-subduction zones and mid-ocean ridges: Implications for H₂O storage and recycling in the mantle. *Earth and Planetary Science Letters*, 137(1-4), 45-55. doi:http://dx.doi.org/10.1016/0012-821X(95)00203-O
- Tenner, T. J., Hirschmann, M. M., Withers, A. C., & Hervig, R. L. (2009). Hydrogen partitioning between nominally anhydrous upper mantle minerals and melt between 3 and 5 GPa and applications to hydrous peridotite partial melting. *Chemical Geology*, 262(1), 42-56.
- Tommasi, A., & Ishikawa, A. (2014). Microstructures, composition, and seismic properties of the Ontong Java Plateau mantle root. *Geochemistry, Geophysics, Geosystems*, 15(11), 4547-4569.
- Whitmeyer, S. J., & Karlstrom, K. E. (2007). Tectonic model for the Proterozoic growth of North America. *Geosphere*, 3(4), 220-259.
- Yang, X. Z., Deloule, E., Xia, Q. K., Fan, Q. C., & Feng, M. (2008). Water contrast between Precambrian and Phanerozoic continental lower crust in eastern China. *Journal of Geophysical Research: Solid Earth*, 113(B8).
- Zhao, Y.-H., Ginsberg, S., & Kohlstedt, D. (2004). Solubility of hydrogen in olivine: dependence on temperature and iron content. *Contributions to Mineralogy and Petrology*, 147(2), 155-161.